# Slip-stimulated grain boundary sliding in Ti-6Al-4 V at room temperature

Samuel Hémery, Christophe Tromas, Patrick Villechaise

Version of Record: https://www.sciencedirect.com/science/article/pii/S2589152918302291
Manuscript_b5fcfdc33fb106f8b464e0df22350958

# Slip-stimulated grain boundary sliding in Ti-6Al-4V at room temperature

Samuel Hémery[1,*], Christophe Tromas[2], Patrick Villechaise[1]

[1] Institut Pprime, CNRS – ENSMA – Université de Poitiers, UPR CNRS 3346, Physics and Mechanics of Materials Department, ISAE-ENSMA – Téléport 2, 1 avenue Clément Ader, BP 40109, 86961 Futuroscope Chasseneuil Cedex, France

[2] Institut Pprime, CNRS – ENSMA – Université de Poitiers, UPR CNRS 3346, Physics and Mechanics of Materials Department, BP 30179, 86962 Futuroscope-Chasseneuil Cedex, France

[*] Corresponding author: samuel.hemery@ensma.fr

**Abstract**

Grain boundary sliding has a substantial contribution to high temperature deformation of α/β titanium alloys. Despite the low homologous temperature, the operation of grain boundary sliding is presently reported at room temperature using a pre-deformed Ti-6Al-4V specimen. Scanning electron microscopy and atomic force microscopy observations were combined with electron back-scattered diffraction characterization in order to to clarify the underlying mechanisms. Intragranular prismatic slip seemingly triggers grain boundary sliding. The analysis of activated slip systems while accounting for crystallographic aspects unveiled several highly influential parameters. Notably, strain partitioning, as a result of plastic anisotropy and microstructural heterogeneities, promotes grain boundary sliding. The orientation of the incident slip band relative to the boundary plane was also found correlated with the occurrence of grain boundary sliding. These findings lay the foundations for identification of conditions favoring grain boundary sliding in titanium alloys and highlight an enriched panel of possible interactions between slip bands and grain boundaries that is likely to play a critical role in crack initiation processes.

**Graphical abstract**

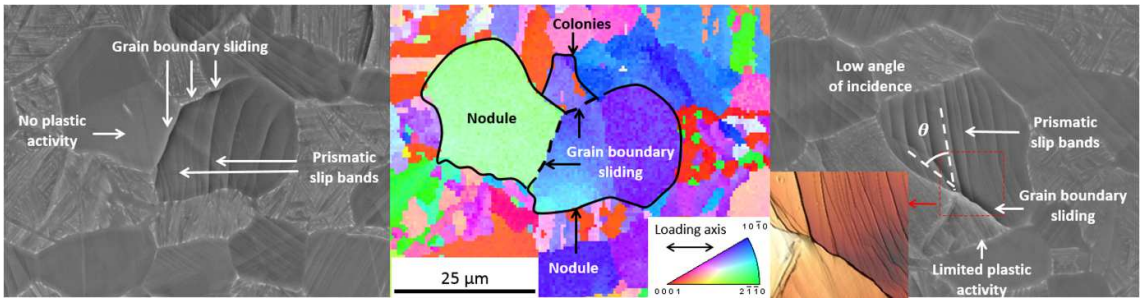


**Keywords: Grain boundary sliding; slip; titanium alloy; crystallographic orientation; plasticity**

## Introduction

Deformation processes operating in α/β titanium alloys have received a lot of interest owing to important industrial applications such as structural aircraft components or disks and blades of gas turbine engines. Among the numerous possible deformation processes encountered in hexagonal closed packed metals, slip is the main deformation system of the α phase at room temperature [1]. 5 types of slip systems have been previously reported: 3 basal slip systems $\{0001\}[11\bar{2}0]$, 3 prismatic slip systems $\{10\bar{1}0\}[11\bar{2}0]$, 6 <a>-type pyramidal slip systems $\{10\bar{1}1\}[11\bar{2}0]$, 6 <c+a>-first order pyramidal slip systems $\{10\bar{1}1\}[11\bar{2}3]$ and 12 <c+a>-second order pyramidal slip systems $\{11\bar{2}2\}[11\bar{2}3]$. The complexity of the deformation behavior at the microstructure scale is increased by significant differences in critical resolved shear stress (CRSS) values associated with the different slip modes. Notably, basal and prismatic slip systems are well-identified as easy deformation modes [2-4]. As a result, grains with a [0001] direction closely aligned to the tensile axis are often designated as 'hard' grains, owing to the difficulty to trigger <c+a>-pyramidal slip activity [5-7]. This plastic anisotropy has major consequences on the alloy performance through strain and stress partitioning under cyclic loadings [8-10]. However, fatigue performance prediction in relation to microstructure, which is critical for most industrial applications, is still a challenging issue.

The fatigue lifetime of titanium alloys is mainly limited by the crack initiation stage [11]. According to prior studies, a restricted number of cracks initiate in very specific arrangements containing the weakest microstructural link [12,13]. This characteristic contributes to a significant variability in the fatigue life of titanium alloys [13,14]. In this context, rare or secondary deformation processes might play a key role in the final properties. Their influence might either be straightforward, if involved in the crack initiation process, or indirect through stress / strain redistribution that either promotes or delays crack initiation. However, they have received much less attention than the slip systems formerly enumerated. For instance, deformation twinning has been recently reported in Ti-6Al-4V at room temperature under monotonic [3] and cyclic loadings [15].

Grain boundary sliding is an alternative deformation process mainly observed at high temperature and / or in fine grained materials. This is a major deformation mode of titanium alloys at intermediate and high temperature [3], including the regime of superplasticity [16-18]. However, the occurrence of grain boundary sliding has been reported at room temperature in several hexagonal close packed metals such as zinc [19] or magnesium and its alloys [20-22]. Several observations of grain boundary sliding have also been reported in commercial purity α titanium [23,24] and along α/β interfaces in a near-β titanium alloy at room temperature [25]. To the best of the authors' knowledge, similar investigations have never been carried out on α/β titanium alloys at room temperature. This is the purpose of the present work.

The occurrence of grain boundary sliding along the interface between primary α nodules and their surrounding (i.e. α nodules or α/β colonies) was investigated using surface observation of a pre-strained specimen with scanning electron microscopy (SEM) and atomic force microscopy (AFM). In order to identify conditions favoring its occurrence, as well as the underlying mechanisms, crystallographic aspects were considered using Electron Back-Scattered Diffraction (EBSD) and interactions with other deformation processes were examined using slip trace analysis.

## Experiments

Ti-6Al-4V with a bi-modal microstructure was used in the present work. A SEM micrograph showing the microstructure is presented in figure 1a. The microstructure is composed of primary

alpha nodules with an average diameter of about 13 µm and secondary alpha lamellas embedded in the beta matrix. Primary nodules account for 36 % of the specimen surface. The distribution of crystallographic orientations relative to the tensile axis obtained from EBSD data is plotted on an inverse pole figure (IPF) in figure 1b. The maximum of 1.9 indicates a weak crystallographic texture. Typical yield stress and tensile strength at a strain rate of $10^{-4}$ $s^{-1}$ are about 913 MPa and 976 MPa respectively. The corresponding elongation is about 17%.

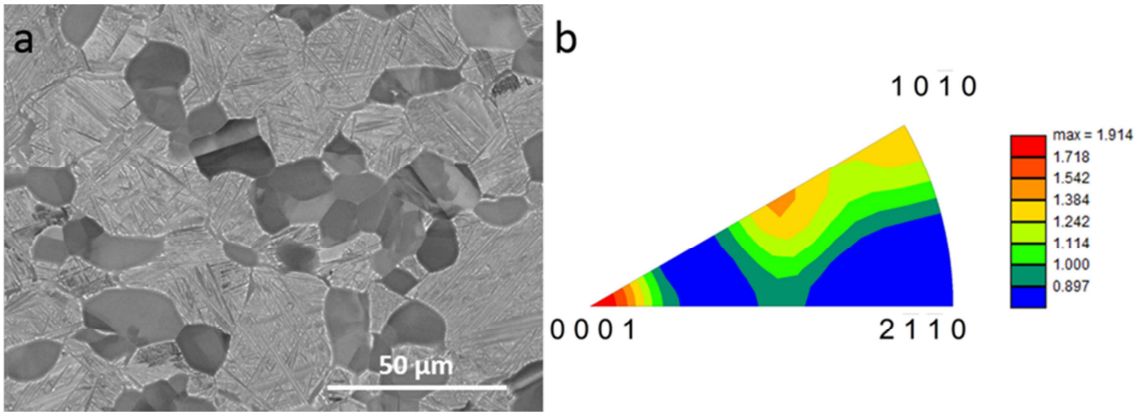


**Figure 1: a. SEM micrograph of the microstructure used in the present work and b. the crystallographic orientation distribution relative to the loading direction plotted on an inverse pole figure**

A 1 mm thick dogbone shaped specimen with a gage length of 10 mm and a gage width of 2 mm was used in the present work. Details of the geometry and dimensions are given in [2]. Both faces of the specimen were first ground finishing with 4000 grade SiC paper. One face was then roughly polished using 9 µm diamond suspension prior to a final polishing step using a mixture of 10 % $H_2O_2$ and 0.04 µm colloidal silica. The mirror finish enables appropriate diffraction conditions for EBSD characterization. Unlike electro-polishing, this procedure also ensures a minimum roughness on the specimen surface, which is essential for a reliable detection of slip traces or ledges associated with grain boundary sliding.

The occurrence of grain boundary sliding was investigated after pre-deformation in tension using a 5 kN Deben tensile stage. A crosshead displacement rate about 0.02 mm/min was applied. The displacement, which is measured using a linear variable differential transformer, was stopped after reaching a plastic strain magnitude of approximately 2.7 %. Surface observations were performed after unloading of the specimen. Although reverse deformation can occur owing to the elastic anisotropy of alpha titanium, no significant difference could be evidenced according to a dedicated in situ SEM tensile test (not shown here for clarity purposes). Hence, no influence is expected on the operation of deformation processes or on the features discussed in the following.

The surface of the specimen was observed using a 6100 JEOL scanning electron microscope. Two regions of 400 x 550 µm² containing a total of 972 nodules were considered. Detection of slip traces and ledges associated with grain boundary sliding was based on topography. As a consequence, slip, or sliding, involving a shear component parallel to the surface might be missed. Both secondary electron (SE) and back-scattered electron (BSE) imaging were used in order to sort out contrasts that may stem from crystallographic orientation or elemental partitioning between different phases. The numerous interfaces in lamellar colonies and the thin beta layers render the distinction between interface sliding and crystallographic slip challenging in such regions. As a consequence, the present work focused on grain boundary sliding involving one or several primary alpha nodules. Furthermore, any doubtful grain boundary sliding case was excluded from the present

analysis. Notably, a limited ledge curvature, or existence of a slip trace in the center of the considered nodule (i.e. away from the boundary) with the same orientation as the boundary suspected of sliding, may induce a difficult distinction between boundary sliding and slip traces. This procedure implies that the reported number of grain boundary sliding observations constitutes a lower bound of the grain boundary sliding occurrences.

The local crystallographic orientation in the regions of interest was characterized using the EBSD technique. A JEOL 6100 SEM equipped with an EBSD setup provided by EDAX was employed. Owing to the low fraction of β phase retained at room temperature [2], only the α phase was considered in the present analysis. A square step of 0.5 µm was applied in order to accurately characterize the crystallographic orientation in primary α nodules. The TSL OIM Analysis software was used to process EBSD data. The average crystallographic orientation of primary α nodules was calculated using the single orientation per grain function and a 5° misorientation criterion. A careful clean up using the grains dilation function with a grain tolerance angle of 5 ° and a minimum grain size of 3 pixels was applied in order to plot the inverse pole figure maps presented in the following. Color coding is relative to the loading direction.

Slip traces analysis was performed in order to investigate a potential relation between operative slip modes and the occurrence of grain boundary sliding. The experimentally observed slip traces were compared to theoretical slip traces calculated for the basal, prismatic and first-order pyramidal planes using grain averaged Euler angles computed from EBSD data. A 5° criterion was applied in order to associate an experimental slip trace with the theoretical trace of a potential slip plane. Multiple - or a lack of - matching traces resulted in a dismissed analysis of the slip trace. Since the slip trace analysis only indicates the slip plane, several assumptions were made for slip system identification. If the slip trace matches the basal plane trace, the basal slip system with the highest Schmid factor was assumed to be active. If the slip trace matches a $\{10\bar{1}1\}$ plane trace, <a>-type pyramidal slip was assumed to be active. Indeed, several studies reported a higher CRSS for <c+a>-type pyramidal slip than for <a>-type pyramidal slip [9,26-28].

In addition to the statistically significant study using SEM, smaller regions where grain boundary sliding occurred were characterized using atomic force microscopy (AFM). Surface topography scans were performed in tapping mode using a Brucker Dimension 3100 AFM and the WSXM software [29] was utilized for topography signal analysis.

## Results

*Phenomenology of grain boundary sliding in Ti-6Al-4V*

According to SEM characterization, 52 grain boundary sliding occurrences have been identified in the region of interest. An example is shown in the micrograph presented in figure 2a. The ledge at the interface between the primary α nodule and its surrounding demonstrates the operation of grain boundary sliding at room temperature in α/β titanium alloys. The sliding process seems insensitive to the microstructure on both sides of the boundary since it proceeds between alpha nodules as well as between lamellar colonies and alpha nodules. 8 grain boundary sliding cases out of 52 cases occurred between primary alpha nodules. In spite of the low associated frequency (≈ 15 %), which is probably related to the surface fraction of primary alpha nodules (≈ 36 %), this observation confirms the weak influence of the microstructure. The inverse pole figure map shown in figure 2b depicts the local crystallographic orientation of the region presented in figure 2a. Since grain boundary sliding extends continuously along the interface between multiple nodules and

colonies with distinct orientations, the crystallographic orientations on both sides of the sliding boundary do not appear as a highly influential parameter as well. However, although grain boundary sliding occasionally involves multiple microstructural elements on one side of the boundary, a single nodule was always noticed on the other side of the boundary. This analysis suggests that characteristics of these nodules may control grain boundary sliding in α/β titanium alloys.

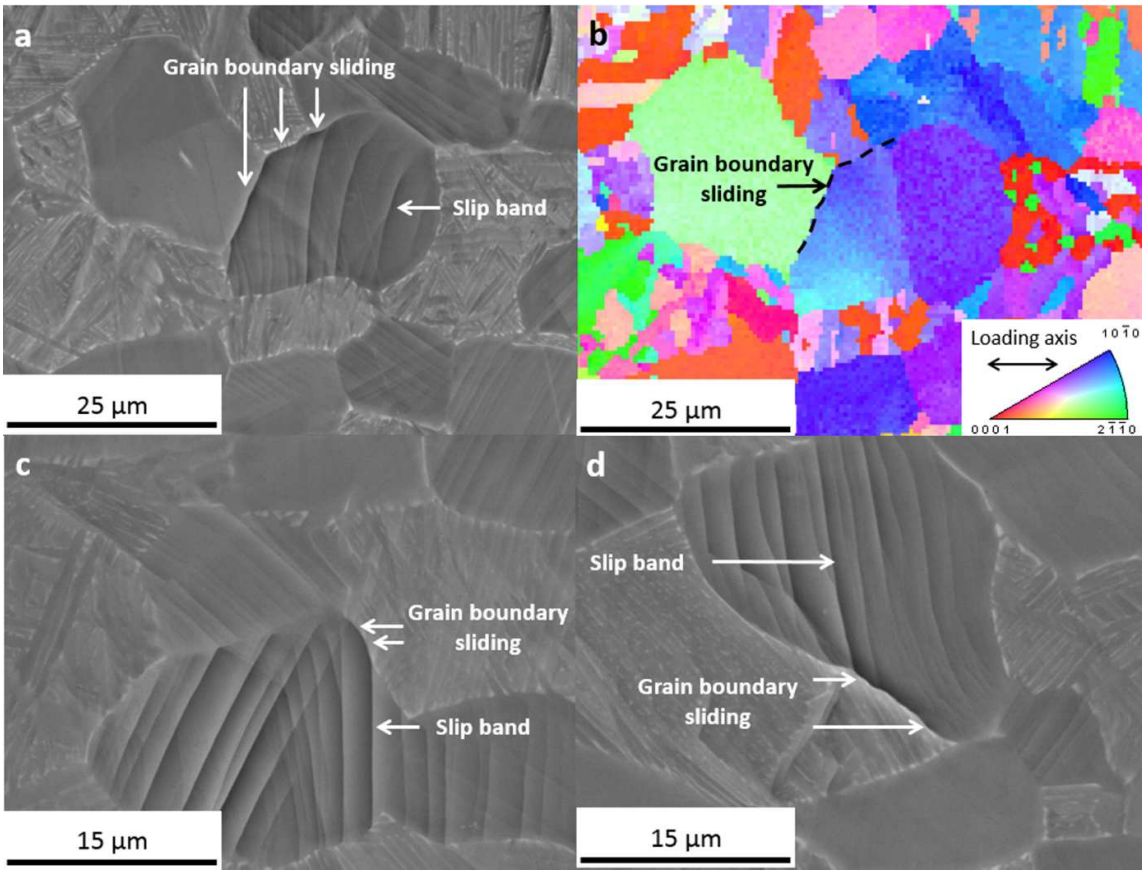


**Figure 2: a. SEM micrograph showing grain boundary sliding extending continuously along the interface with multiple nodules and colonies, b. the associated inverse pole figure maps showing the local crystallographic orientation, c. and d. SEM micrographs showing slip induced grain boundary sliding**

In particular, these nodules invariably exhibit slip traces. In most cases (47 out of 52 cases), an incoming slip band intersects the sliding boundary. Typical examples are shown in figure 2c and 2d. A decrease in the slip step height near the boundary due to dislocations piling up might be expected [30]. A careful examination of the micrographs shown in figures 2c and 2d suggests a different behavior near the sliding boundary. The slip step height associated with the incoming slip band rather seems to be nearly maximum near the boundary. Concurrently, the grain boundary ledge height suddenly increases at the intersection of the slip band with the boundary.

In order to confirm this analysis, several sliding grain boundaries were observed using AFM. A typical example is presented and discussed in the following. An SEM BSE image of the region surrounding a sliding grain boundary is shown in figure 3a. Intense slip traces are noticed in the nodule involved in grain boundary sliding. Theoretical slip traces as calculated using EBSD data are indicated for basal, prismatic and pyramidal planes. The experimental slip traces correspond to a prismatic slip system with a Schmid factor of 0.482. This value is the maximum Schmid factor among basal, prismatic and pyramidal slip systems. As stated above, examination of the interaction between

the incoming slip bands and the upper boundary suggests that grain boundary sliding is triggered by intragranular slip. A detailed AFM image showing the topography of the region surrounding the nodule is presented in figure 3b. Magnified views of the upper and lower boundaries with different orientations are shown in figure c and d respectively. No grain boundary ledge is noticed on the left of the a' marker. In contrast a ledge reveals sliding of the boundary on the right of the a' marker. Near the intersection between the slip trace and the boundary, the magnitude of the step heights appears similar for the incoming slip band and the sliding boundary. The height on the edge of 3 slip bands was quantified. The profiles are reported in figure 3 e. All 3 profiles (a – a', b – b' and c – c') show a saturation near the upper boundary, where the height is maximum. In contrast, the height profiles show a decrease near the lower boundary. This observation reveals dislocation pile-ups. However, the slip step height do not reach zero near the lower grain boundary. This indicates that a significant number of dislocations are absorbed by the lower boundary despite the fact that no grain boundary sliding could be detected. A few sharp drops, which are associated with cross-slip, are noticed on the a – a' and b – b' profiles. Cross-slip is usually considered as inhibited by short range order in titanium alloys with a high aluminum content. However, a previous study reported the observation of cross-slip only in large dislocation pile-ups, where dislocation motion is impeded by the high density of dislocations in the slip plane [31].

According to the previous observations, grain boundary sliding seems tightly related with intragranular slip. The next paragraphs deal with this characteristic.

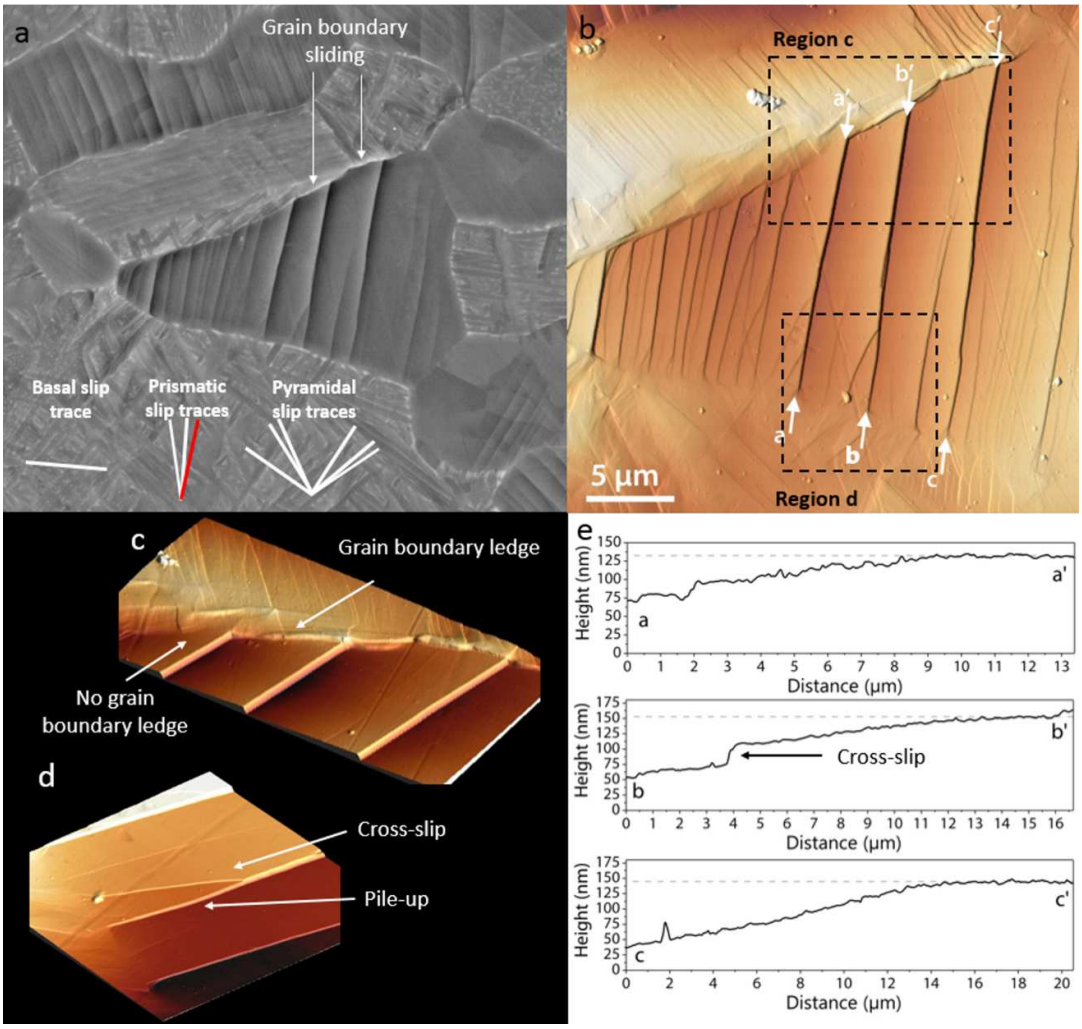


**Figure 3 a. BSE-SEM micrograph showing a nodule with a sliding boundary (the slip traces associated with potential slip systems in the nodule are also indicated), b. tapping mode AFM observation of the same region (topography image in 3D top view), c., d. magnifications of near boundary regions with a different orientation (topography image in 3D) and e. height profile along the edge of 3 slip lines**

*Intragranular slip mode associated with grain boundary sliding*

A potential relation between the active slip mode and the occurrence of grain boundary sliding was then investigated. Since the main slip modes involved in deformation of titanium alloys correspond to distinct crystallographic orientation domains [2-4,32,33], the crystallographic orientation of nodules associated with grain boundary sliding was first studied. The crystallographic orientation of a) all the nodules in the region of interest, b) nodules exhibiting slip traces and c) nodules associated with grain boundary sliding are plotted on inverse pole figures in figure 4. Considering all nodules, the figure 3a presents a homogenous distribution of the crystallographic orientations over the whole orientation domain. As shown in figure 3b, the crystallographic orientation of nodules with slip traces is also fairly well distributed despite a slightly lower density near the (0001) pole. Nodules with the [0001] direction closely aligned with the tensile axis are difficult to deform owing to low resolved shear stresses on basal and prismatic slip systems and the high critical resolved shear stress for <c+a>-pyramidal slip activation. Conversely, the crystallographic

orientations of nodules associated with grain boundary sliding are gathered in a restricted orientation domain, which roughly corresponds to an angle between the c-axis of the hexagonal closed packed lattice and the loading direction in the 45° - 90° interval. According to prior studies, this orientation domain corresponds to high prismatic Schmid Factors as well as prismatic slip activity [2-4,32,33].

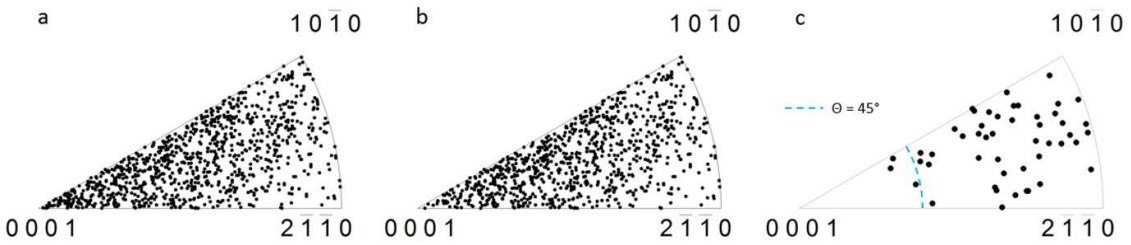


**Figure 4: Crystallographic orientation relative to the loading direction plotted on inverse pole figures of a. all nodules, b. nodules exhibiting slip traces and c. nodules associated with grain boundary sliding**

Basal and prismatic Schmid factors were computed for each nodule associated with grain boundary sliding. Since basal and prismatic slip exhibit similar strength for Ti alloys with 6 wt. % Al and Schmid's law was found to provide a fair insight into the activated slip systems [2,4,27], the slip system with the maximum Schmid factor among basal and prismatic slip systems was assumed to be active. The maximum Schmid factor and the corresponding slip mode are reported in table 1 for each nodule associated with grain boundary sliding. Among the 52 nodules, the maximum Schmid factor corresponds to a prismatic slip system for 41 nodules (79 %) and to a basal slip system for 11 nodules (21 %). Accordingly, prismatic slip seems more prone to trigger grain boundary sliding. However, the following question remains: Is basal slip able to trigger grain boundary sliding?

| Nodule | Euler angles | | | Maximum basal / prismatic SF | | Slip trace analysis | | | | | | | |
|---|---|---|---|---|---|---|---|---|---|---|---|---|---|
| N° | Phi 1 | PHI | Phi 2 | Slip mode | Maximum SF | Slip mode 1 | SF 1 | Slip mode 2 | SF 2 | Slip mode 3 | SF 3 | Slip mode 4 | SF 4 |
| 1 | 106 | 72.8 | 273.1 | P | 0.451 | Pyr | 0.492 | X | X | - | - | - | - |
| 2 | 83.3 | 89.8 | 286.3 | P | 0.493 | P | X | - | - | - | - | - | - |
| 3 | 225.5 | 71.3 | 119 | B | 0.471 | X | X | X | X | - | - | - | - |
| 4 | 236 | 54.2 | 124.8 | P | 0.396 | X | X | - | - | - | - | - | - |
| 5 | 191.1 | 44.9 | 173.1 | B | 0.465 | Pyr | 0.410 | X | X | X | X | - | - |
| 6 | 259.8 | 82.9 | 80.4 | P | 0.480 | X | X | - | - | - | - | - | - |
| 7 | 93.8 | 87.2 | 253.2 | P | 0.497 | P | X | - | - | - | - | - | - |
| 8 | 277.6 | 53.4 | 75.8 | P | 0.486 | P | 0.486 | - | - | - | - | - | - |
| 9 | 265.1 | 84.9 | 98.5 | P | 0.482 | P | 0.482 | - | - | - | - | - | - |
| 10 | 94.1 | 77.2 | 271.2 | P | 0.448 | P | 0.448 | - | - | - | - | - | - |
| 11 | 90.9 | 83.9 | 278.7 | P | 0.488 | P | X | - | - | - | - | - | - |
| 12 | 296.6 | 64.4 | 42.8 | P | 0.393 | P | 0.320 | X | X | - | - | - | - |
| 13 | 77.5 | 76.8 | 290.6 | P | 0.476 | P | X | - | - | - | - | - | - |
| 14 | 88.7 | 55.9 | 284.4 | P | 0.499 | P | 0.499 | - | - | - | - | - | - |
| 15 | 245.8 | 87.3 | 115.2 | P | 0.396 | P | 0.309 | - | - | - | - | - | - |
| 16 | 190.1 | 53 | 164.6 | B | 0.425 | X | X | - | - | - | - | - | - |
| 17 | 256.5 | 73.7 | 88.8 | P | 0.447 | X | X | - | - | - | - | - | - |
| 18 | 281.9 | 58.6 | 74.7 | P | 0.474 | X | X | - | - | - | - | - | - |
| 19 | 70.8 | 59.1 | 314.7 | P | 0.430 | P | 0.430 | P | 0.357 | - | - | - | - |
| 20 | 71.2 | 61.3 | 299.2 | P | 0.453 | X | X | X | X | - | - | - | - |
| 21 | 293.8 | 80.3 | 85.9 | P | 0.366 | Pyr | 0.472 | Pyr | 0.471 | - | - | - | - |
| 22 | 283.3 | 78.5 | 62.8 | P | 0.449 | P | 0.298 | X | X | - | - | - | - |
| 23 | 88.9 | 77.5 | 285.5 | P | 0.500 | P | 0.500 | - | - | - | - | - | - |
| 24 | 62.6 | 59.2 | 283.9 | P | 0.372 | Pyr | 0.476 | X | X | - | - | - | - |
| 25 | 250.2 | 53.8 | 127.7 | P | 0.431 | P | 0.431 | - | - | - | - | - | - |
| 26 | 70.8 | 84.3 | 298.5 | P | 0.411 | P | 0.357 | - | - | - | - | - | - |
| 27 | 118.3 | 68.2 | 244 | P | 0.403 | P | 0.403 | - | - | - | - | - | - |
| 28 | 17.8 | 45.5 | 7.4 | B | 0.498 | B | 0.498 | P | 0.222 | - | - | - | - |
| 29 | 207.5 | 54.6 | 176.4 | B | 0.494 | X | X | - | - | - | - | - | - |
| 30 | 267.9 | 59.1 | 68.5 | P | 0.482 | P | 0.482 | P | 0.354 | - | - | - | - |
| 31 | 112 | 84.9 | 241.1 | P | 0.394 | P | 0.347 | - | - | - | - | - | - |
| 32 | 264.3 | 55.3 | 108 | P | 0.497 | P | 0.497 | - | - | - | - | - | - |
| 33 | 132.5 | 46.2 | 231.4 | B | 0.390 | X | X | - | - | - | - | - | - |
| 34 | 28.3 | 24.7 | 338.2 | P | 0.422 | P | 0.422 | B | 0.319 | - | - | - | - |
| 35 | 359.9 | 53.6 | 9.3 | B | 0.446 | B | 0.446 | Pyr | 0.317 | P | 0.172 | X | X |
| 36 | 294.6 | 67.2 | 49.7 | P | 0.371 | P | 0.368 | Pyr | 0.173 | - | - | - | - |

| | | | | | | | | | | | | | |
|---|---|---|---|---|---|---|---|---|---|---|---|---|---|
| 37 | 282.8 | 70.7 | 71.7 | P | 0.478 | P | 0.478 | - | - | - | - | - | - |
| 38 | 346.8 | 40.9 | 25.1 | B | 0.455 | B | 0.455 | Pyr | 0.438 | - | - | - | - |
| 39 | 284.9 | 70.2 | 85.8 | P | 0.415 | X | X | X | X | - | - | - | - |
| 40 | 34.7 | 38.1 | 321.7 | B | 0.390 | P | 0.340 | - | - | - | - | - | - |
| 41 | 140 | 63.1 | 233.3 | B | 0.464 | B | 0.464 | X | X | - | - | - | - |
| 42 | 57.6 | 51.9 | 298.9 | P | 0.397 | Pyr | 0.070 | - | - | - | - | - | - |
| 43 | 70 | 69 | 272.2 | P | 0.423 | P | 0.423 | - | - | - | - | - | - |
| 44 | 67.4 | 77.8 | 318.7 | P | 0.429 | P | 0.429 | - | - | - | - | - | - |
| 45 | 115.5 | 69.7 | 259.1 | P | 0.373 | Pyr | 0.464 | P | 0.022 | - | - | - | - |
| 46 | 99.5 | 78.2 | 252.6 | P | 0.487 | P | 0.487 | - | - | - | - | - | - |
| 47 | 246.7 | 90.9 | 95.3 | P | 0.400 | X | X | - | - | - | - | - | - |
| 48 | 275.4 | 86.7 | 77.5 | P | 0.493 | P | X | - | - | - | - | - | - |
| 49 | 317.1 | 67.9 | 62.6 | B | 0.453 | B | 0.453 | P | 0.050 | - | - | - | - |
| 50 | 104.1 | 81.7 | 272.5 | P | 0.440 | X | X | - | - | - | - | - | - |
| 51 | 243 | 53 | 146.8 | P | 0.427 | P | 0.427 | B | 0.333 | - | - | - | - |
| 52 | 117.2 | 83.8 | 221.2 | P | 0.397 | B | 0.390 | Pyr | 0.216 | - | - | - | - |

**Table 1: Number of nodules associated with grain boundary sliding and the corresponding Euler angles, slip mode and Schmid factor (SF) associated with the slip system exhibiting the maximum Schmid factor among basal and prismatic slip systems and activated slip systems identified using a slip trace analysis (X: Slip traces not matching with an identified slip system, -: No other observable slip trace)**

The slip traces on the 52 nodules associated with grain boundary sliding were analyzed. The slip mode and the Schmid factor of successfully identified slip traces are reported in table 1. A significant fraction of slip traces could not be confidently assigned to a slip system for the following reasons: multiple theoretical traces matched the experimental one in a 5° interval, no theoretical trace could match the experimental one in a 5° interval and/or slip traces are occasionally curved as illustrated in figure 2 a. Unidentified slip traces, which do not match the successfully identified ones, are also indicated by a cross in table 1. Despite the presence of slip traces on the surface of all nodules, the variable number of activated slip systems (between 1 and 4) in each nodule hints a heterogeneous deformation behavior. The active slip modes in nodules associated with grain boundary sliding were carefully examined. The following observations were made.

Firstly, nodules with a maximum Schmid factor associated with basal slip most often exhibit additional prismatic, pyramidal or unidentified slip traces that do not match the basal plane trace. Only one nodule associated with grain boundary sliding presents solely basal slip traces on its surface. However, slip underneath the specimen surface or leading to insufficiently high slip steps to be detected cannot be excluded. According to this analysis, a potential implication of basal slip in grain boundary sliding could not be demonstrated.

Secondly, 11 nodules exhibit slip traces associated with pyramidal planes versus 8 nodules for the basal plane and 34 for prismatic planes. Slip traces analysis carried out in prior studies showed that less than 10 % of nodules exhibit pyramidal slip traces. In the present work, pyramidal slip traces account for 21 % of the successfully identified slip systems. This unexpectedly high value might be related to a higher plastic strain magnitude than most of prior studies, as well as the preferential orientation of nodules associated with grain boundary sliding, which implies a moderate to high pyramidal Schmid factor [2]. However, only nodule 42 exhibits solely pyramidal slip traces. In contrast, 23 nodules exhibit only prismatic slip traces. This shows the straightforward relation existing between prismatic slip and grain boundary sliding. However, another question arises: Why are all the nodules experiencing prismatic slip mediated deformation not associated with grain boundary sliding?

*Orientation of slip bands relative to the grain boundary plane*

Although microstructure reconstruction techniques such as focused ion beam offer insights into investigating the 3D geometry of grain boundaries [34-37], this task is still experimentally challenging when considering statistically significant data. Owing to this constraint, the orientation of

the incident slip band relative to the sliding boundary was studied using surface observations. The angle between the slip trace and the boundary trace, denoted as θ in the following, was measured for each grain boundary sliding occurrence. A diagram illustrating θ measurement on a grain boundary sliding case is presented in figure 5a. Unfortunately, a few sliding boundaries are not apparently intersected by slip traces. An example is shown in figure 2a. As a result, 42 angle measurements were extracted from the 52 grain boundary sliding cases. The associated frequencies are plotted in figure 4b using 10 ° intervals. The maximum frequency is located within the 30 ° - 40 ° interval. However, a bias is introduced by the applied procedure. A good alignment between grain boundary ledges and slip traces on the surface of the nodule, which might lead to a confusion between slip traces and grain boundary ledges, resulted in an exclusion from the present analysis. As a consequence, low angle magnitudes between the slip traces and the boundary traces are underrepresented in these distributions.

A reference frequency distribution was required to highlight a potential influence of the angle between the incident slip band and the boundary on grain boundary sliding occurrence. Two alternative approaches have been applied in order to rule out any bias. The first distribution is based on the measurement of the angle between 200 randomly selected slip traces and the intercepted boundary traces. The associated frequency distribution is plotted in figure 5b using 10 ° intervals. The data were split into sets of 50 or 100 values and the corresponding frequency distributions (not shown here for clarity purposes) were not significantly different from the one shown in figure 4b. This suggests that the amount of slip traces presently considered seems fairly representative. However, a systematic bias could be introduced by the manual selection of the slip bands.

A second distribution based on a 2D simplified geometric model was employed in order to rule out this potential bias. Round nodules containing *N* slip traces with a constant $\frac{D}{N-1}$ spacing with *D* the nodule diameter were considered as an approximation. The angle between the *k* slip trace and the boundary was calculated analytically for each slip trace using the following formula: $\theta = \cos^{-1}\frac{2k}{N-1}$ with *k=0* at the center of the nodule. A schematic representation is shown in figure 5 c. 79 slip bands were considered in order to obtain a smooth frequency distribution. The associated frequencies are plotted in figure 5 b using 10 ° intervals.

Both reference distributions (i.e. based on randomly selected slip bands or the 2D geometric model) are very similar. The maximum frequency is located within the 80 ° – 90 ° interval. The frequency decreases with decreasing incidence angle. The slight differences in the magnitude of the frequencies are most likely related to bias introduced by the present approaches such as i) manual selection of slip traces which may not lead to a perfectly representative distribution, or ii) the round nodule geometry or the constant slip band spacing approximations used in the geometric model, which depict idealized microstructure and deformation distribution as shown in the micrographs of figure 2. However, the frequency distribution associated with grain boundary sliding is strikingly different from both reference distributions. Notably, the maximum frequency is met in the 30 ° - 40 ° interval in contrast to the 80 ° - 90 ° interval for the reference distributions. Hence, slip bands with a low angle of incidence seem more prone to induce grain boundary sliding.

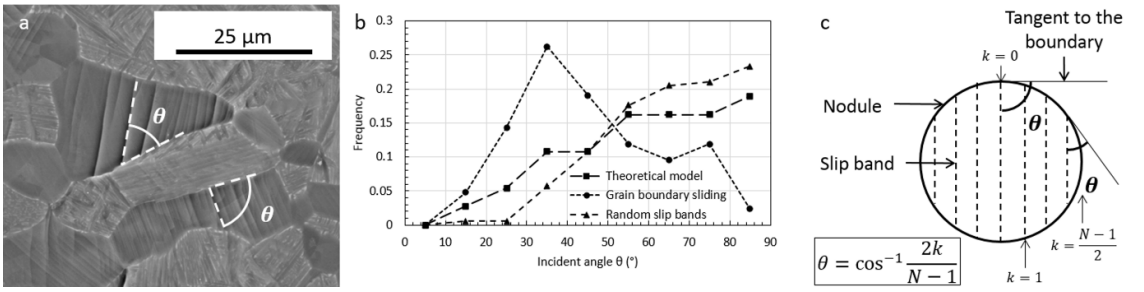


**Figure 5: a. Micrograph showing the angle (θ) between the trace corresponding to the incident slip band and the nodule boundary trace, b. frequency distribution of the incident angle (θ) for grain boundary sliding cases, random slip traces selection and the geometrical model and c. diagram showing the calculation of θ in a round nodule according to geometric considerations**

## Discussion

Grain boundary sliding was presently evidenced as an operating deformation process in Ti-6Al-4V at room temperature. 52 grain boundary sliding occurrences have been identified. The regions of interest contain about 972 nodules including 875 nodules with slip traces. Considering the applied procedure and the involved hypothesis, at least 5 % of nodules and 6 % of nodules with slip traces are associated with grain boundary sliding. These values are most likely tightly related to the stress / strain state, the crystallographic texture, the characterization technique, etc. However, similar orders of magnitude were found for pyramidal <a> slip, pyramidal <c+a> slip and twinning in Ti-6Al-4V at room temperature [3], revealing that this deformation process is not rare and should be considered for advanced micromechanical modeling or mechanistic investigations.

Two accommodation processes associated with grain boundary sliding are described in the literature: diffusion [38] and slip [39]. In the first place, dislocation accommodation would be expected for Ti-6Al-4V tested at room temperature, since the phenomena of vacancy diffusion and dislocation climb are less likely than at higher temperatures. The present observations revealed a tight relation between grain boundary sliding and intragranular slip, which is a well-known factor promoting grain boundary sliding [40]. Grain boundary shear, which is generated by slip activity, is accommodated by grain boundary sliding. In titanium alloys such as Ti-6Al-4V, dislocations are emitted from α/β interfaces [41]. Hence, grain boundary sliding may result from dislocation absorption by the boundary as well as from shearing of the boundary induced by dislocation emission from the interface.

The crystallographic orientation of nodules associated with grain boundary sliding and the intragranular slip traces were analyzed, unambiguously proving that prismatic slip is involved in grain boundary sliding. The ability of basal and pyramidal slip to trigger grain boundary sliding could not be demonstrated. Although basal and pyramidal slip might be involved in a restricted number of cases, a prismatic slip activity underneath the specimen surface cannot be excluded. Further investigations, such as characterization of dislocation structures using a combination of focused ion beam lift outs and transmission electron microscopy, are mandatory to clarify this point. This approach could also help to shed light on the potential role of the β layers that can be locally retained at boundaries. Indeed, prior studies reported the occurrence of grain boundary sliding at α/β interface [25]. In addition, investigations at high temperature suggested an easier sliding along α/β interfaces than along α/α or β/β interfaces [17]. The potential role of β layers is not clear yet for Ti-6Al-4V at room temperature.

Since grain boundary sliding was observed along boundaries between nodules and between nodules and colonies, the microstructural elements surrounding the boundary do not appear as of prime influence on the occurrence of grain boundary sliding. However, Mussot and his co-workers showed that internal stresses induced by strain incompatibilities facilitate grain boundary sliding activation [42]. About 90 % of grain boundary sliding occurrences involve a nodule with slip traces on its surface and a surrounding, on the other side of the sliding boundary, without any slip trace detected using SEM. This observation suggests a marked effect of strain partitioning. At the microstructural scale, plastic strain heterogeneities result from intrinsic anisotropy of hexagonal close packed α titanium and microstructural heterogeneities. 44 out of 52 grain boundary sliding cases involved a deforming nodule and a colony. This observation is probably related to the low surface fraction of primary alpha nodules (≈ 36 %). However, another contribution has to be accounted for. Owing to a reduced slip length, the critical resolved shear stress for slip activation is higher in lamellar colonies than in nodules [2,43]. As a consequence, more strain incompatibilities might be expected at boundaries between nodules and colonies boundaries than at the boundaries between nodules. This analysis suggests a potential effect of the alloy microstructure on grain boundary sliding occurrence.

The occurrence of grain boundary sliding seems also facilitated if the incident slip bands exhibit a low misorientation with the grain boundary plane. The consequences are twofold: i) the boundary is likely to experience a significant resolved shear stress, which is a major factor for grain boundary sliding [44], ii) grain boundary sliding might be facilitated by a good geometric alignment between the incoming slip band and the boundary (i.e. similarly to slip transfer [45]). These points merit further investigation in order to clarify their respective importance.

Based on SEM observations and high angular resolution EBSD analysis of deformed commercial purity titanium, Guo and his co-workers identified some slip bands that lead to neither stress concentration nor slip transfer [46]. The authors suspected the absorption of lattice dislocations onto the grain boundary and motion of grain boundary dislocations ahead of blocked slip bands generating local grain boundary sliding. According to prior studies [47,48], the stress concentration resulting from slip band / grain boundary interactions are involved in crack initiation under monotonic or cyclic loadings. The occurrence of grain boundary sliding is likely to affect local stress fields and may reduce the magnitude of stress concentrations. Hence, this mode of deformation has to be considered for prediction of crack initiation sites, but could also be used to improve the fatigue / dwell-fatigue performance of titanium alloys.

**Conclusions**

The occurrence of grain boundary sliding was observed at room temperature in Ti-6Al-4V with a bimodal microstructure. An analysis based on a statistically significant number of observations revealed that grain boundary sliding has to be considered as a deformation mode in α/β titanium alloys. The following key findings provide the basis for prediction and understanding of grain boundary sliding occurrence:

- Although the operation of grain boundary sliding has seemingly no direct relation with the surrounding microstructure (i.e. nodule / nodule or nodule / colony), intragranular slip activity appears as mandatory.
- In particular, prismatic slip seems to be key while the implication of basal and pyramidal slip, associated with rare observations, could not be demonstrated.

- In agreement with prior studies, grain boundary sliding seems promoted by local plastic anisotropy and deformation heterogeneities. In this way, bi-modal microstructures may favor its occurrence.
- A low angle between the incident slip band and the boundary seems favorable to trigger grain boundary sliding. Further investigations are required to clarify whether a high resolved shear stress acting on the grain boundary, a good geometric alignment or both are needed.

**Declaration of interest** - None

**Acknowledgements**

A. Cervellon is acknowledged for proof reading the manuscript.

**References**

[1] G. Lütjering, J.C. Williams, Titanium, 2nd edition, Springer, Berlin; New York, 2007.

[2] F. Bridier, P. Villechaise, J. Mendez, Analysis of the different slip systems activated by tension in a α/β titanium alloy in relation with local crystallographic orientation, Acta Mater. 53 (2005) 555–567.

[3] H. Li, C.J. Boehlert, T.R. Bieler, M.A. Crimp, Examination of the distribution of the tensile deformation systems in tension and tension-creep of Ti-6Al-4V (wt.%) at 296 K and 728 K, Philos. Mag. 95 (2015) 691–729.

[4] S. Hémery, P. Villechaise, On the influence of ageing on the onset of plastic slip in Ti-6Al-4V at room temperature: Insight on dwell fatigue behavior, Scripta Mater. 130 (2017) 157–160.

[5]J.R. Mayeur, D.L. McDowell, A three-dimensional crystal plasticity model for duplex Ti–6Al–4V, Int. J. Plasticity 23 (2007) 1457–1485.

[6] J.L.W. Warwick, J. Coakley, S.L. Raghunathan, R.J. Talling, D. Dye, Effect of texture on load partitioning in Ti-6Al-4V, Acta Mater. 60 (2012) 4117–4127.

[7] H. Li, D.E. Mason, T.R. Bieler, C.J. Boehlert, M.A. Crimp, Methodology for estimating the critical resolved shear stress ratios of α-phase Ti using EBSD-based trace analysis, Acta Mater. 61 (2013) 7555–7567.

[8] M.R. Bache, Processing titanium alloys for optimum fatigue performance, Int. J. Fatigue 21 (1999) 105–111.

[9] V. Hasija, S. Ghosh, M.J. Mills, D.S. Joseph, Deformation and creep modeling in polycrystalline Ti–6Al alloys, Acta Mater. 51 (2003) 4533–4549.

[10] F.P.E. Dunne, D. Rugg, A. Walker, Lengthscale-dependent, elastically anisotropic, physically-based hcp crystal plasticity: Application to cold-dwell fatigue in Ti alloys, Int. J. Plasticity 23 (2007) 1061–1083.

[11] J.A. Hall, Fatigue crack initiation in alpha-beta titanium alloys, Int. J. Fatigue 19 (1997) 23–37.

[12] F.P.E. Dunne, D. Rugg, On the mechanisms of fatigue facet nucleation in titanium alloys, Fat. Fract. Eng. M. 31 (2008) 949–958.

[13] S.K. Jha, C.J. Szczepanski, P.J. Golden, W.J. Porter, R. John, Characterization of fatigue crack-initiation facets in relation to lifetime variability in Ti–6Al–4V, Int. J. Fatigue. 42 (2012) 248–257.

[14] S.K. Jha, C.J. Szczepanski, R. John, J.M. Larsen, Deformation heterogeneities and their role in life-limiting fatigue failures in a two-phase titanium alloy, Acta Mater. 82 (2015) 378–395.

[15] C. Lavogiez, S. Hémery, P. Villechaise, Concurrent operation of ⟨c + a⟩ slip and twinning under cyclic loading of Ti-6Al-4V, Scripta Mater. 157 (2018) 30–33.

[16] A. Arieli, A. Rosen, Superplastic deformation of Ti-6Al-4V alloy, Metall. Trans. A 8 (1977) 1591–1596.

[17] J.S. Kim, Y.W. Chang, C.S. Lee, Quantitative analysis on boundary sliding and its accommodation mode during superplastic deformation of two-phase Ti-6Al-4V alloy, Metall. Mater. Trans. A 29 (1998) 217–226.

[18] E. Alabort, D. Putman, R.C.Reed, Superplasticity in Ti–6Al–4V: Characterisation, modelling and applications, Acta Mater. 95 (2015) 428–442.

[19] T. Matsunaga, T. Kameyama, S. Ueda, E. Sato, Grain boundary sliding during ambient-temperature creep in hexagonal close-packed metals, Philos. Mag. 90 (2010) 4041–4054.

[20] J. Koike, R. Ohyama, T. Kobayashi, M. Suzuki, K. Maruyama, Grain-Boundary Sliding in AZ31 Magnesium Alloys at Room Temperature to 523 K, Mater. Trans. 44 (2003) 445–451.

[21] J. Koike, Enhanced deformation mechanisms by anisotropic plasticity in polycrystalline Mg alloys at room temperature, Metall. Mater. Trans. A 36 (2005) 1689–1696.

[22] N. Stanford, K. Sotoudeh, P.S. Bate, Deformation mechanisms and plastic anisotropy in magnesium alloy AZ31, Acta Mater. 59 (2011) 4866–4874.

[23] T.R. Bieler, M.A. Crimp, Y. Yang, L. Wang, P. Eisenlohr, D.E. Mason, W. Liu, G.E. Ice, Strain heterogeneity and damage nucleation at grain boundaries during monotonic deformation in commercial purity titanium, JOM 61 (2009) 45–52.

[24] V. Doquet, B. Barkia, Combined AFM, SEM and crystal plasticity analysis of grain boundary sliding in titanium at room temperature, Mech. Mater. 103 (2016) 18–27.

[25] S. Ankem, H. Margolin, Alpha-Beta Interface Sliding in Ti-Mn Alloys, Metall. Trans. 14 (1983) 500–503.

[26] I.P. Jones, W.B. Hutchinson, Stress-state dependence of slip in Titanium-6Al-4V and other H.C.P. metals, Acta Metall. 29 (1981) 951–968.

[27] J.C. Williams, R.G. Baggerly, N.E. Paton, Deformation behavior of HCP Ti-Al alloy single crystals, Metall. Mater. Trans. A 33 (2002) 837–850.

[28] S. Zaefferer, A study of active deformation systems in titanium alloys: dependence on alloy composition and correlation with deformation texture, Mater. Sci. Eng.: A-Struct. 344 (2003) 20–30.

[29] I. Horcas, R. Fernández, J.M. Gómez-Rodríguez, J. Colchero, J. Gómez-Herrero, A.M. Baro, WSXM: a software for scanning probe microscopy and a tool for nanotechnology, Rev. Sci. Instrum. 78 (2007) 013705.

[30] K. Jagannadham, R.W. Armstrong, Evidence for dislocation pile-ups at grain boundaries from slip band step height observations, Scripta Metall. 21 (1987) 1459–1462.

[31] P. Castany, F. Pettinari-Sturmel, J. Douin, A. Coujou, TEM quantitative characterization of short-range order and its effects on the deformation micromechanims in a Ti-6Al-4V alloy, Mater. Sci. Eng.: A-Struct. 680 (2017) 85–91.

[32] M.P. Echlin, J.C. Stinville, V.M. Miller, W.C. Lenthe, T.M. Pollock, Incipient slip and long range plastic strain localization in microtextured Ti-6Al-4V titanium, Acta Mater. 114 (2016) 164–175.

[33] S. Hémery, V.T. Dang, L. Signor, P. Villechaise, Influence of Microtexture on Early Plastic Slip Activity in Ti-6Al-4V Polycrystals, Metall. Mater. Trans. A (2018) 1–9.

[34] M.D. Uchic, M.A. Groeber, A.D. Rollett, Automated serial sectioning methods for rapid collection of 3-D microstructure data, JOM 63 (2011) 25–29.

[35] M.P. Echlin, M. Straw, S. Randolph, J. Filevich, T.M. Pollock, The TriBeam system: Femtosecond laser ablation in situ SEM, Mater. Charact. 100 (2015) 1–12.

[36] Y. Su, C. Zambaldi, D. Mercier, P. Eisenlohr, T.R. Bieler, M.A. Crimp, Quantifying deformation processes near grain boundaries in α titanium using nanoindentation and crystal plasticity modeling, Int. J. Plasticity 86 (2016) 170–186.

[37] R. Ding, J. Gong, A.J. Wilkinson, I.P. Jones, A study of dislocation transmission through a grain boundary in hcp Ti–6Al using micro-cantilevers, Acta Mater. 103 (2016) 416–423.

[38] M.F. Ashby, R.A. Verrall, Diffusion-accommodated flow and superplasticity, Acta Metall. 21 (1973) 149–163.

[39] A. Ball, Superplasticity in the aluminium-zinc eutectoid—an early model revisited, Mater. Sci. Eng.: A-Struct. 234–236 (1997) 365–369.

[40] L. Priester, Grain Boundaries and Crystalline Plasticity, John Wiley & Sons, London, 2011.

[41] P. Castany, F. Pettinari-Sturmel, J. Crestou, J. Douin, A. Coujou, Experimental study of dislocation mobility in a Ti–6Al–4V alloy, Acta Mater. 55 (2007) 6284–6291.

[42] P. Mussot, C. Rey, A. Zaoui, grain boundary sliding and strain compatibility, Res. Mech. 14 (1985) 69-79.

[43] S. Hémery, P. Villechaise, Investigation of Size Effects in Slip Strength of Titanium Alloys: Alpha Nodule Size Dependence of the Critical Resolved Shear Stress, Metall. Mater. Trans. A. (2018) 1–4.

[44] R.C. Gifkins, A. Gittins, R.L. Bell, T.G. Langdon, The dependence of grain-boundary sliding on shear stress, J. Mater. Sci. 3 (1968) 306–313.

[45] S. Hémery, P. Nizou, P. Villechaise, In situ SEM investigation of slip transfer in Ti-6Al-4V: Effect of applied stress, Mater. Sci. Eng.: A-Struct. 709 (2018) 277–284.

[46] Y. Guo, T.B. Britton, A.J. Wilkinson, Slip band–grain boundary interactions in commercial-purity titanium, Acta Mater. 76 (2014) 1–12.

[47] W.J. Evans, M.R. Bache, Dwell-sensitive fatigue under biaxial loads in the near-alpha titanium alloy IMI685, Int. J. Fat. 16 (1994) 443–452.

[48] Z. Yan, K. Wang, Y. Zhou, X. Zhu, R. Xin, Q. Liu, Crystallographic orientation dependent crack nucleation during the compression of a widmannstätten-structure α/β titanium alloy, Scripta Materialia. 156 (2018) 110–114.